NUMERICAL SIMULATION OF EFFECTS OF GENERATION OF SOLITONS MOVING A REGION OF SURFACE PRESSURE

B. E. Protopopov

UDC 532.59

During motion over a fluid surface of a pressure localization region with a nearly critical velocity (the Froude number is close to unity in depth) one may observe an interesting phenomenon: along with the generation of the wake of the wave the perturbation source (the moving pressure region) generates periodically a soliton-shape wave, escaping from it above the flow, and emerging from the regime of motion with constant (supercritical) velocity without changing its shape.

The effect described of soliton generation, initially observed experimentally, was subsequently verified by numerical calculations. This was first done in [1], where the Boussinesq approximation was used, generalized to the case of presence of a surface pressure. The model includes both nonlinear and dispersion effects (in whose interaction is also shaped the mechanism of the given effect), making it possible to obtain an adequate qualitative pattern of the process. However, due to the approximate nature of the model, constructed under the assumption of smallness of dispersion and nonlinearity, the problem arises of validity of the quantitative results. Another approximate model, applicable to the study of soliton generation and induced by the Korteweg–de Vries equation [2] is even less general, since it is a further approximation of the Boussinesq approximation to the case in which the perturbation source moves with a velocity near the critical velocity. Some idea about the extent of verifiability of the approximate modeling of the given process can be obtained from [3], where calculation results of both models were compared, and comparison with experiment was also carried out for generation of solitons moving over a rough bottom.

In the present paper the effect of soliton generation is considered within a more general model of potential flow of an ideal incompressible fluid, free of the restrictions on amplitude and length of the waves investigated. The dependence of the basic process characteristics on surface pressure intensity is analyzed numerically. In that case, along with the potential model we investigate a generalized Boussinesq model, with the purpose of estimating the validity limits of the latter.

1. It is assumed that at some moment of time the region occupied by the fluid is a curvilinear quadrilateral $Q(t) = \{0 \le x \le \ell, -h \le y \le \eta(x, t)\}$ in a Cartesian coordinate system Oxy with axes x and y directed along the surface level of the unperturbed fluid and vertically above, respectively. The fluid motion occurs under the action of an external force – an assigned surface pressure distribution $p(x, t)$. Consider the case in which the pressure is concentrated on a bounded support, and varies with time as a whole:

$$p(x, t) = p_0(\xi) = \begin{cases} p_m f(\xi) & \text{for} \quad |\xi| \leqslant 1, \\ 0 & \text{for} \quad |\xi| > 1, \end{cases} \tag{1.1}$$

where $\xi = x - X(t)$ is the local coordinate, $x = X(t)$ is the given law of motion of the mean point $\xi = 0$ of the pressure region, $p_m = \text{const}$, and $\max f(\xi) = 1$. Here and in what follows we use only dimensionless variables, and the scales of all quantities are selected in such a manner that the semilength of the surface pressure, the free fall acceleration, and the fluid density are equal to unity.

Novosibirsk. Translated from Zhurnal Prikladnoi Mekhaniki i Tekhnicheskoi Fiziki, No. 3, pp. 78-84, May-June, 1991. Original article submitted November 30, 1989.

0021-8944/91/3203-0371$12.50

To describe the fluid motion we use the potential flow model of an ideal fluid and the generalized Boussinesq approximation. In this and other models the corresponding system contains two equations of evolutionary type, one of which describing the time variation of the shape of the fluid surface $\eta(x, t)$, and the other necessary for determining the evolution of the velocity field. Formally they can be written down in general form for both models

$$\eta_t + v = 0; \tag{1.2}$$

$$q_t + s_x = 0 \tag{1.3}$$

with functions v(x, t), q(x, t), s(x, t). The equations written are supplemented by initial value

$$\eta = \eta_0(x), \; q = q_0(x) \text{ for } t = 0 \tag{1.4}$$

and additional relations between η, v, q, s, closing the system.

Within the potential model these relations are

$$q = u; \tag{1.5}$$

$$s = \frac{1}{1+\eta_x^2}\left(\frac{1}{2}(u^2 - v^2) + \eta_x uv\right) + \eta + p. \tag{1.6}$$

Here u(x, t) and v(x, t) are the tangential and normal components (accurately within a normalization factor) of the velocity vector of fluid particles, found at the surface $y = \eta(x, t)$. According to [4], v is determined as a result of action of the normal derivative operator N on the boundary value potential $\varphi = \varphi(x, t)$: $v = N\varphi$, where

$$\varphi(x, t) = \varphi_0(t) + \int_0^x u(\xi, t)\, d\xi \tag{1.7}$$

with an arbitrary function $\varphi_0(t)$. The action of the nonlocal operator $N(\eta)$ is defined as

$$N\varphi = \eta_x \Phi_x - \Phi_y \text{ for } y = \eta(x, t). \tag{1.8}$$

Here $\Phi(x, y, t)$ is the solution of the elliptic problem

$$\Phi_{xx} + \Phi_{yy} = 0 \text{ in } Q(t), \; \Phi_x = 0 \text{ for } x = 0, \; x = l,$$
$$\Phi_y = 0 \text{ for } y = -h, \; \Phi = \varphi \text{ for } y = \eta(x, t).$$

The required function $\eta(x, t)$ determines one of the boundary regions Q(t), generating several difficulties in solving the elliptic problem. The variable replacement $(x, y, t) \to (x, z, t)$ $(z = (\eta - y)/(\eta + h))$ is used to overcome them. The flow region Q(t) of this replacement is transformed to the constant quadrilateral $\Pi = \{0 \le x \le \ell, \; 0 \le z \le 1\}$. In the new variables the elliptic problem acquires the form

$$U_x + V_z = 0 \text{ in } \Pi; \tag{1.9}$$

$$U = 0 \text{ for } x = 0, \; x = l; \tag{1.10}$$

$$V = 0 \text{ for } z = 1; \tag{1.11}$$

$$\Phi = \varphi \text{ for } z = 0. \tag{1.12}$$

The following notations were used here:

$$U(x,\ z,\ t) = \alpha\Phi_x + \beta\Phi_z,\ V(x,\ z,\ t) = \beta\Phi_x + \gamma\Phi_z; \tag{1.13}$$

$$\alpha(x,\ t) = \eta + h,\ \beta(x,\ z,\ t) = (1 - z)\eta_x,\ \gamma(x,\ z,\ t) = (1 + \beta^2)/\alpha. \tag{1.14}$$

In completing the statement of the problem within the potential model, relation (1.8) is rewritten:

$$v = V_l \text{ for } z = 0. \tag{1.15}$$

In the generalized Boussinesq model the system of equations (1.2)-(1.4) is closed substantially more simply [1]:

$$q = w - (1/3)h^2 w_{xx}; \tag{1.16}$$

$$w = 0 \text{ for } x = 0,\ x = l; \tag{1.17}$$

$$s = (1/2)w^2 + \eta + p,\ v = [(\eta + h)w]_x \tag{1.18}$$

[w(x, t) is the horizontal velocity component averaged over depth]. The relative simplicity of the generalized Boussinesq approximation [the systems of equations (1.2)-(1.4), (1.16)-(1.18)] in comparison with the potential model [the system (1.2)-(1.7), (1.9)-(1.15)] is achieved due to the restrictions on the amplitude a and length λ of the investigated waves [1]:

$$\delta_1 = a/h \ll 1,\quad \delta_2 = h/\lambda \ll 1,\quad \delta_1 = O(\delta_2^2). \tag{1.19}$$

2. The numerical solution algorithm of the problem, both within the potential model and within the Boussinesq approximation, is constructed by the finite difference method. The evolutionary equations are approximated by the Crank–Nicholson scheme with second order in t:

$$\eta^{n+1,k+1} = \eta^n - \frac{\tau}{2}(v^{n+1,k} + v^n);\quad q^{n+1,k+1} = q^n - \frac{\tau}{2}(s_x^{n+1,k} + s_x^n)$$

(τ is the step in time, the first superscript is the step number in time, and the second is the iteration number). The iteration process at each step in t is necessary due to the implicitness of the scheme and the nonlinearity of the supplementary relations in η, v, q, s.

In the potential model, in parallel with the iteration of nonlinear terms a reconstruction is realized of the solution of the elliptic problem by the scheme of stabilizing corrections (the first subscript is omitted):

$$\Phi^{k+1/2} - \omega U_x^{k+1/2} = \Phi^k + \omega V_z^k; \tag{2.1}$$

$$U^{k+1/2} = (\Phi_x^{k+1/2} + \beta^{k+1}V^k)/\gamma^{k+1}; \tag{2.2}$$

$$U^{k+1/2} = 0 \text{ for } x = 0,\ x = l; \tag{2.3}$$

$$\Phi^{k+1} - \omega V_z^{k+1} = \Phi^{k+1/2} - \omega V_z^k; \tag{2.4}$$

$$V^{k+1} = (\Phi_z^{k+1} + \beta^{k+1}U^{k+1/2})/\alpha^{k+1}; \tag{2.5}$$

$$\Phi^{k+1} = \varphi^{k+1} \text{ for } z = 0,\ V^{k+1} = 0 \text{ for } z = 1 \tag{2.6}$$

(ω is an iteration parameter).

The derivatives with respect to spatial variables are approximated in both models by second order, while for this purpose one uses only symmetric differences, which is possible due to the appearance of spaced lattice sites for the various functions. At the points $x_{i-1/2}$, where $x_\nu = \nu h_1$ ($h_1 = l/m_1$ is the grid step in the variable x, and m_1 is an integer) are located the nodes $\eta_{i-1/2} = \eta(x_{i-1/2}, t)$, $v_{i-1/2}$, $s_{i-1/2}$ ($i = 1, \ldots, m_1$), and between these points are the nodes q_i ($i = 1, \ldots, m_1 - 1$). Also at the points x_i, but including also the ends of the segment [0, l], are located the nodes u_i or w_i ($i = 0, \ldots, m_1$).

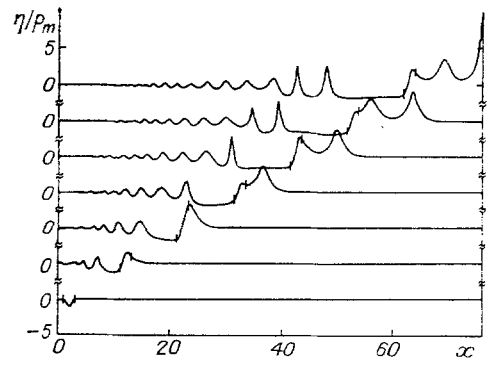

Fig. 1

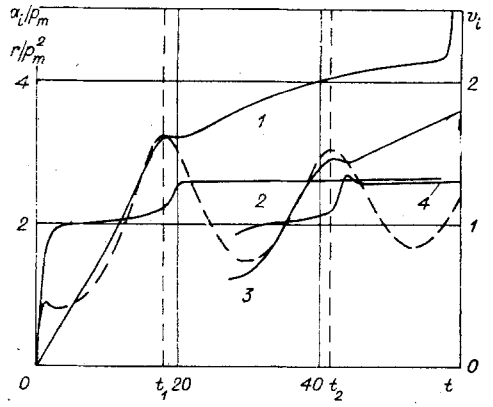

Fig. 2

Within the potential model the elliptic problem (2.1)-(2.6) is calculated on a grid consisting of the nodes $\Phi_{i-1/2,j-1} = \Phi(x_{i-1/2}, z_{j-1}, t)$ ($i = 1, \ldots, m_1$, $j = 1, \ldots, m_2$), $U_{i,j-1}$ ($i = 0, \ldots, m_1$, $j = 1, \ldots, m_2$), $V_{i-1/2,j-1/2}$ ($i = 1, \ldots, m_1$, $j = 0, \ldots, m_2$), where $z_\nu = \nu h_2$ ($h_2 = 1/(m_2 - 0.5)$ is the step over the coordinate z, and m_2 is an integer). Following the replacement of derivatives by corresponding similar differences, the solution of the system of equations (2.1)-(2.6) reduces to inversion of a sequence of tridiagonal matrices. A more detailed description of the computational algorithm of the elliptic problem can be found in [5].

Within the Boussinesq approximation the elliptic part of the problem, represented by Eq. (1.16) with boundary conditions (1.17), is quite simple, and its finite-difference realization is obvious.

3. In the calculations we used the following parameter values, determining the flow geometry: channel length $\ell = 75$, and width $h = 1$. The pressure is distributed over its carrier according to (1.1) with the function $f(\xi) = (1/2)(1 + \cos\pi\xi)$. The maximum pressure value p_m was varied. The law of motion of source perturbation was given in the form

$$X(t) = \begin{cases} x_0 & \text{for} \quad t \leqslant 0, \\ x_0 + ct & \text{for} \quad t > 0 \end{cases} \tag{3.1}$$

with starting point $x_0 = 2$ and constant velocity $c = 1$, which is critical in selecting the channel width: $Fr = c/\sqrt{h} = 1$. Until the initial moment of motion of the pressure region the fluid is at rest, i.e., $\eta_0(x) = -p_0(x - x_0)$, $q_0(x) \equiv 0$.

The calculation results by the potential model in the case $p_m = 0.2$ with grid parameters $m_1 = 375$, $m_2 = 10$, $\tau/h_1 = 0.5$ are presented in Figs. 1 and 2. Figure 1 shows the wave profile evolution. The lower curve is the shape of the fluid surface at $t = 0$, and further above are the profiles through equal time segments $\Delta t = 10$ until the final computing time $t = 60$. At each curve the two vertical primes denote the portion of the surface at which the pressure is nonvanishing at the given moment of time. Figure 1 demonstrates smoothly the formation process of solitons, traveling ahead from the perturbation source in the direction of its motion (above the flow, in a reference system attached to the pressure region). Two such solitons manage to get formed by the moment $t = 60$, the first of which (the top curve) is already found in a phase of collapse at the right wall. The fluid discharge at soliton formation is compensated by formation of a longitudinal cavity at the surface behind the perturbation source.

The evolution of the solitons generated with time can be followed from Fig. 2, where the variations in their amplitudes and velocities are shown. Curve 1 is the amplitude $a_1(t)$ of the first soliton, more accurately, the vertical coordinate of the local maximum of the fluid surface ahead of the perturbation source, and 2 is the velocity of motion $v_1(t)$ of this maximum, i.e., the time derivative of its horizontal coordinate. At some moment of time and in front of the pressure region is generated a certain local maximum, the variations of whose amplitude $a_2(t)$ and velocity $v_2(t)$ are shown by curves 3 and 4, respectively. The dashed line in Fig. 2 shows the wave resistance r(t) [1]:

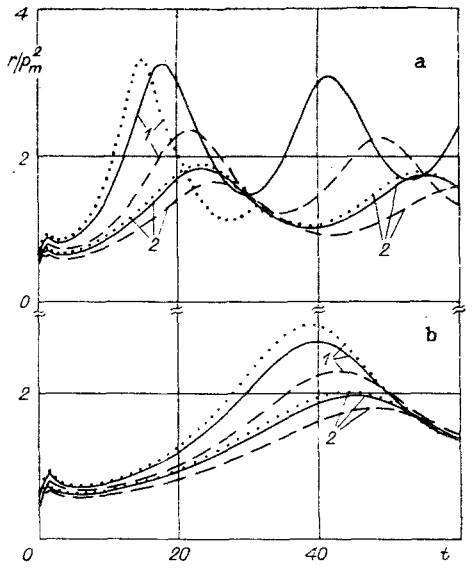

Fig. 3

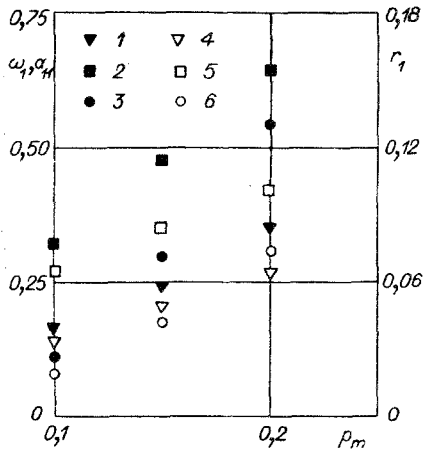

Fig. 4

$$r(t) = \int_0^l p\eta_x \, dx.$$

The separation of the i-th (i = 1, 2, ...) soliton from the perturbation source is manifested in the nonmonotonic behavior of the corresponding curve $a_i(t)$, the sharp increase in $v_i(t)$, and achievement of an alternate local maximum of the function r(t). The maximum points of r(t) are naturally assumed to be the soliton separation moments. As seen from Fig. 2, each separated soliton moves ahead with almost constant velocity, while its amplitude continues increasing (with a reduced pace).

The dependence of the fundamental characteristics of the process investigated (the soliton generation frequencies, their amplitudes and wave resistance) on the intensity of external action on the fluid is of interest. In the given case the distribution $f(\xi)$ and the velocity of motion of the pressure region c are assumed fixed, so that the parameter p_m serves as a measure of intensity. According to investigation results in approximate models [2, 3], with increasing p_m one must expect an increase in the soliton generation frequencies, as well as their amplitudes and velocities, which is verified by the data of the present calculations. In that case only a quite narrow range of p_m variation (approximately from 0.1 to 0.2) is suitable for effective numerical investigation of the process, in the sense that assigning p_m from this interval guarantees an acceptable frequency of soliton generation (i.e., a quite fast evolution process) and moderate values of the amplitudes of solitons and waves generated in the medium, not leading to development of instabilities.

The dependences of the fundamental process characteristics on the pressure intensity p_m, varied within the limits mentioned, are shown in Figs. 3 and 4, allowing, besides, to trace the dynamics of divergence of calculation results according to the Boussinesq approximation with potential model results with increasing p_m, i.e., with enhanced process nonlinearity [increasing parameters δ_1, δ_2 of (1.19)]. Figure 3 provides the wave resistance r(t), calculated for $p_m = 0.2$(a) and 0.1(b). The solid, primed, and dotted lines 1 correspond to calculations by the potential flow model of an ideal fluid, and the similar lines 2 correspond to the generalized Boussinesq approximation. The basic variant of the calculation with a grid step along the horizontal coordinate $h_1 = 0.2$ is shown by solid curves, while the solid and dotted curves are the calculation results with $h_1 = 0.4$ and $h_1 = 0.1$, respectively. For variation of the grid step along the horizontal coordinate the ratio $\tau/h_1 = 0.5$ and the step value $h_2 = 2/19$ along z have remained unchanged.

The frequency values calculated by the potential model for the occurrence of the first soliton $\omega_1 = 2\pi/t_1$, its amplitude $a_{11} = a_1(t_1)$, and the wave resistance $r_1 = r(t_1)$ at the moment of time t_1 are shown as a function of p_m in Fig. 4 by the points 1-3, respectively, while the points 4-6 are the values of the same parameters, found as a result of a calcula-

tion by the generalized Boussinesq approximation. It can be seen that for $p_m = 0.2$ the approximate model, compared to the more accurate potential model, reduces substantially the soliton generation frequency (by 25%), their amplitudes at the moment of separation (by 35%), and the maximum value of the wave resistance (by 43%). With decreasing p_m the deviations between the data obtained within the models considered decrease, and for $p_m = 0.1$ the relative errors in the quantities listed above are 11, 16, and 28%. By an uncomplicated extrapolation over the results shown in Fig. 4 one can obtain the upper limit p_m^* of the interval of variation in p_m, by which using the generalized Boussinesq approximation leads to errors not exceeding 10% (relative to calculation results by the potential model), in all process parameters considered here: $p_m^* = 0.04$.

4. As a measure of controlling the calculation accuracy we provide a verification of the process of fluid mass conservation; more precisely, we followed the variation in time of the integral

$$\Delta M(t) = \int_0^l (\eta(x, t) - \eta_0(x))\, dx.$$

At the end moment of the calculation t = 60 (600 steps in time) the mass defect $\Delta M(t)$ reached $8.3 \cdot 10^{-5}$ for $p_m = 0.1$ and $6.5 \cdot 10^{-5}$ for $p_m = 0.2$. For the Boussinesq approximation these numbers are substantially better: $1.4 \cdot 10^{-9}$ and $3.4 \cdot 10^{-9}$, respectively, but even the value $8.3 \cdot 10^{-5}$ must be considered fully satisfactory, taking into account that the whole fluid mass in the channel is approximately $h\ell = 75$. The fluid mass conservation in potential model calculations can be improved by increasing the number of iterations at each step in t, i.e., due to increasing cost in computer time for the indicated values of mass defect this cost is also high due to the two-dimensionality of the elliptic part of the problem, substantially exceeding (by 50 times for $p_m = 0.1$ and by almost 100 times for $p_m = 0.2$) the similar cost when using the generalized Boussinesq approximation.

With the purpose of analyzing the sensitivity of the numerical experiment results to variation of the grid parameters we carried out control calculations with step variations along the horizontal coordinate $h_1 = \{0.4, 0.2, 0.1\}$ and in time (while retaining the ratio $\tau/h_1 = 0.5$). The step in the z coordinate in the potential model remained unchanged ($h_2 = 2/19$). From Fig. 3 one can trace the effect of grid parameter variation on the behavior of the wave resistance. On the whole the reduction in computational grid provides a qualitative effect, similar to the effect of increasing p_m, i.e., an enhancement of nonlinearity – an increase in the soliton generation frequencies and in their amplitudes. This effect is natural, since it reflects the reduction in computational discrepancy with decreasing grid step. As to the magnitude of this effect, i.e., the relative variations in the various flow characteristics during transition from one grid to another, then in the potential model, as compared with the Boussinesq approximation, these vriations seem, firstly, more noticeable in the whole interval $0.1 \leq p_m \leq 0.2$, and, secondly, they depend substantially on p_m. Thus, for $p_m = 0.1$ the deviation between the potential and approximate models in the first soliton amplitude at its moment of separation were 14, 16, and 17% at grids with $h_1 = 0.4$, 0.2, and 0.1, respectively, and for $p_m = 0.2$ – 21, 35, and 44%. Thus, with increasing p_m an accurate numerical investigation of the process becomes quite difficult, not only due to the impossibility of validating the approximate, weakly nonlinear models, but also due to the necessity of using quite small computational grids in numerical solution of equations, accurately accounting for the nonlinearity.

The author is grateful to I. V. Sturov for stating the problem and for his interest in this study.

LITERATURE CITED

1. D. M. Wu and T. Y. Wu, "Three-dimensional nonlinear long waves due to moving surface pressure," Proc. 14th Symp. Naval Hydrodynamics, Michigan (1982).
2. T. Y. Wu, "Generation of upstream advancing solitons by moving disturbances," J. Fluid Mech., 184, 75 (1987).
3. S. J. Lee, G. T. Yates, and T. Y. Wu, "Experiments and analyses of upstream-advancing solitary-waves generated by moving disturbances," J. Fluid Mech., 199, 563 (1989).
4. L. V. Ovsyannikov, N. I. Makarenko, V. I. Nalimov, et al., Nonlinear Problems in the Theory of Surface and Internal Waves [in Russian], Nauka, Novosibirsk (1985).

5. B. E. Protopopov, "Numerical simulation of surface waves in a channel of variable depth," in: Dynamics of Continuous Media [in Russian], Sb. Nauch. Tr. Akad. Nauk SSSR, Sib. Otd., Inst. Gidrodinamiki (1988), No. 84.

SURFACING OF A HEAVY SPHERE IN VIBRATING SAND

B. V. Levin

UDC 531.131

This article reports the results of an experimental study of the motion of a sphere in a vibrating free-flowing medium. Analysis of the results made it possible to establish that the mean upward velocity of the sphere is linearly dependent on its diameter.

The effects of the motion of a uniform, free-flowing vibrating medium in an oscillating field of accelerations comparable to (vibro-fluidization regime) or greater than (vibro-boiling regime) gravitational acceleration with regard to amplitude have been studied in fairly great detail and are being put to use in industry [1]. Several experimental [2] and theoretical [3] studies have examined the surfacing of heavy bodies and immersion of light bodies in a vibrating liquid. Numerical methods were used in conjunction with a two-dimensional model in [4] to study the laws governing the vibrational separation (segregation) of a uniform mixture of particles of two very different diameters. As far as we know, there have not been any experimental studies of the vertical motion of a single sphere in a horizontal layer of a vibrating free-flowing medium. However, this problem is of interest both for technical applications and for geophysics, in connection with the need to investigate the anomalous "surfacing" effects noted in the literature in earthquakes involving the movement of large masses of soil and boulders under fine-grained sedimentary rock [5].

The experiments were conducted on a vibration unit which provided for motion of the free-flowing medium in a variable gravitational field created by vertical oscillations of the vibrator. The unit was a cylindrical container 50 cm in diameter and 20 cm high. Installed in the bottom part of the container was a plane coaxial vibrator 20 cm in diameter (Fig. 1). The vibrator ensured vibration of a layer of dry sand up to 15 cm thick with accelerations up to 25 m/sec^2 and a constant vibration amplitude of 0.1 cm. The frequency of vibration ranged from 1 to 25 Hz. The test sphere was placed at the bottom of the sand layer. After the vibrator was turned on and had operated for a certain period of time at a certain frequency, the sphere ended up on the surface of the sand. The thickness of the sand layer was changed with the range from 4 to 10 cm and was measured in each test both before the vibrator was turned on and after the sphere had risen to the surface. We used spheres ranging in diameter D from 4 to 45 mm. They were made of wood, cork, clay, paraffin, glass, polystyrene, iron, aluminum, and lead.

In the main test series, we recorded the average velocity of the sphere V as the ratio of the thickness of the sand layer to the average time of movement of the sphere from the bottom to the surface measured with a stopwatch. We also studied the law of motion of the sphere with the use of a system (Fig. 1) which included a thin inextensible filament, a lightweight dial gauge, and an extensible elastic filament (to raise the pointer). The use of a system with an elastic filament made it possible to determine the minimum frequency at which the sphere begins to rise and to fix the moment of the beginning of motion and the change in velocity over the initial section of the sphere's path. More than 200 tests were conducted with spheres of different diameters. The error of the determination of velocity in a given measurement was no greater than 5%. The slightly tensioned rubber filament did not significantly distort the measurement results.

The completed tests allowed us to find the threshold frequency at which the sphere surfaces. This value was found to be f_{min} = 20 Hz. The tests also made it possible to fix the initial velocity of the sphere (V_{min} = 0.1 mm/sec) and to study the character of the

Lyubertsy. Translated from Zhurnal Prikladnoi Mekhaniki i Tekhnicheskoi Fiziki, No. 3, pp. 85-87, May-June, 1991. Original article submitted January 26, 1989; revision submitted November 10, 1989.

0021-8944/91/3203-0377$12.50